Geosci. Model Dev. Discuss., 7, 6629–6675, 2014
www.geosci-model-dev-discuss.net/7/6629/2014/
doi:10.5194/gmdd-7-6629-2014

Geoscientific Model Development Discussions
Open Access

Hindcast regional climate simulations within EURO-CORDEX: evaluation of a WRF multi-physics ensemble

E. Katragkou[1], M. García-Díez[2,3], R. Vautard[4], S. Sobolowski[5], P. Zanis[1], G. Alexandri[6], R. M. Cardoso[7], A. Colette[8], J. Fernández[3], A. Gobiet[9], K. Goergen[10,11,12], T. Karacostas[1], S. Knist[11], S. Mayer[5], P. M. M. Soares[7], I. Pytharoulis[1], I. Tegoulias[1], A. Tsikerdekis[1], and D. Jacob[13]

[1]Department of Meteorology and Climatology, School of Geology, Aristotle University of Thessaloniki, Thessaloniki, Greece
[2]Instituto de Física de Cantabria, CSIC-UC, Santander, Spain
[3]Department of Applied Mathematics and Computer Science, Universidad de Cantabria, Santander, Spain
[4]Laboratoire des Sciences du Climat et de l'Environment, IPSL, CEA/CNRS/UVSQ, Gif sur Yvette, France
[5]Uni Research Climate, Bergen, Norway
[6]Laboratory of Atmospheric Physics, School of Physics, Aristotle University of Thessaloniki, Thessaloniki, Greece
[7]Instituto Dom Luiz, Faculdade de Ciências, Universidade de Lisboa, 1749-016 Lisboa, Portugal

[8]Institut National de l' Environment industriel et des risques (INERIS), Verneuil en Halatte, France
[9]Wegener Center for Climate and Global Change, University of Graz, Graz, Austria
[10]Centre de Recherche Public – Gabriel Lippmann, Belvaux, Luxembourg
[11]Meteorological Institute, University of Bonn, Bonn, Germany
[12]Jülich Supercomputing Centre, Forschungszentrum Jülich GmbH, Jülich, Germany
[13]Climate Service Centre, Hamburg, Germany

Received: 5 September 2014 – Accepted: 17 September 2014 – Published: 2 October 2014

Correspondence to: E. Katragkou (katragou@auth.gr)

Published by Copernicus Publications on behalf of the European Geosciences Union.

GMDD
7, 6629–6675, 2014

Abstract

In the current work we present six hindcast Weather Research and Forecasting (WRF) simulations for the EURO-CORDEX domain with different configurations in microphysics, convection and radiation for the time period 1990–2008. All regional model simulations are forced by the ERA-Interim reanalysis and have the same spatial resolution (0.44°). These simulations are evaluated for surface temperature, precipitation, short- and longwave downward radiation at the surface and total cloud cover. The analysis of the WRF ensemble indicates systematic biases in both temperature and precipitation linked to different physical mechanisms for the summer and winter season. Overestimation of total cloud cover and underestimation of downward shortwave radiation at the surface, mostly when using Grell–Devenyi convection and the CAM radiation scheme, intensifies the negative summer temperature bias in northern Europe (max −2.5 °C). Conversely, a strong positive downward shortwave summer bias in central (40–60 %) and southern Europe mitigates the systematic cold bias in WRF over these regions, signifying a typical case of error compensation. Maximum winter cold bias is over north-eastern Europe (−2.8 °C); this location is indicative of land–atmosphere rather than cloud-radiation interactions. Precipitation is systematically overestimated in summer by all model configurations, especially the higher quantiles, which are associated with summertime deep cumulus convection. The Kain–Fritsch convection scheme produces the larger summertime precipitation biases over the Mediterranean. Winter precipitation is reproduced with lower biases by all model configurations (15–30 %). The results of this study indicate the importance of evaluating not only the basic climatic parameters of interest for climate change applications (temperature-precipitation), but also other components of the energy and water cycle, in order to identify the sources of systematic biases, possible compensatory or masking mechanisms and suggest methodologies for model improvement.

GMDD

7, 6629–6675, 2014

1 Introduction

Climate models are the primary tools for investigating the response of the climate system to various forcings, making climate predictions on seasonal to decadal time scales and projections of future climate. Regional climate models (RCMs) are applied over limited-area domains with boundary conditions either from global reanalysis or global climate model output. The use of RCMs for dynamical downscaling has grown, their resolution has increased, process-descriptions have developed further, new components have been added, and coordinated ensemble experiments have become more widespread (Rummukainen, 2010; Flato et al., 2013). A significant constraint in a comprehensive evaluation of regional downscaling is that available studies often employ different methods, regions, periods and observational data for evaluation. Thus, evaluation results are difficult to generalize. The Coordinated Regional Climate Downscaling Experiment (CORDEX) initiative provides a platform for a joint evaluation of model performance, along with a solid scientific basis for impact assessments and other uses of downscaled climate information (Giorgi et al., 2009).

Published work within CORDEX focusing on the European domain (EURO-CORDEX) for present climate, indicates strengths and deficiencies of the state-of-the-art modeling tools, already used to downscale the Coupled Model Intercomparison Project Phase 5 (CMIP5) global model results. Kotlarski et al. (2014), in a joint evaluation based on the EURO-CORDEX RCM ensemble, reported bias ranges for temperature and precipitation corresponding to those of the ENSEMBLES simulations (van der Linden et al., 2009) with some improvements identified and strong influence of specific choices of model configuration on model performance. Vautard et al. (2013), focusing on the European heatwaves with the EURO-CORDEX ensemble, found that high temperature are primarily sensitive to convection and micro-physics. Comparison of the Weather Research and Forecasting model (WRF) (Skamarock et al., 2008) multi-physics ensemble vs. the multi-model EURO-CORDEX ensemble by Garcia-Diez et al. (2014a) suggests that WRF multi-physics and multi-model ensemble spreads

GMDD
7, 6629–6675, 2014

within EURO-CORDEX were of the same order. Giorgi et al. (2012) highlighted the significant sensitivity of model performance on different parameterization schemes and parameter settings in a RegCM4 model study over different CORDEX domains including Europe.

These findings indicate that combining model evaluation with sensitivity studies is necessary in order to investigate recurring and persistent biases, list potential sources of their origin, dissuade/encourage modelers from using specific configuration responsible for systematic errors over specific regions and suggest tracks for model development. Since large model ensemble spreads and present climate biases are potentially linked with future climate uncertainties (Boberg and Christensen., 2012), it is important to understand contributions of individual processes on the present European climate in order to be able to interpret future climate projections with greater confidence and possibly constrain these projections (Hall and Qu, 2006; Stegehuis et al., 2013).

In the current work we analyze hindcast simulations of the WRF multi-physics ensemble performed within the framework of EURO-CORDEX. Recent research has demonstrated the ability to use WRF to refine global climate modeling results to higher spatial resolutions in Europe (e.g. Soares et al., 2012; Cardoso et al., 2013; Warrach-Sagi et al., 2013). The aim of this study is to identify systematic biases and areas of large uncertainties in present European climate and relate them to specific physical processes (e.g. cloud-radiation or land–atmosphere interactions). This analysis contributes towards a better understanding of WRF as a dynamical downscaling tool for RCM modeling studies and its optimization for this specific region.

2 Data and methodology

2.1 Observations

To evaluate the model simulations we use daily mean temperature and precipitation values from E-OBS version 9.0 (hereafter EOBS9) covering the area 25–75° N and

GMDD
7, 6629–6675, 2014

40° W–75° E, available on a 0.44° rotated pole grid (Haylock et al., 2008). The E-OBS dataset is based on the ECA&D (European Climate Assessment and Data) station dataset and other stations from different archives.

Short- and longwave downwelling radiation fluxes at the surface and cloud fraction were evaluated with the International Satellite Cloud Climatology Project (ISCCP) Flux Dataset. The ISCCP radiation fluxes comprise a satellite derived product including shortwave (0.2–5 µm) and longwave (5.0–200 µm) radiation at the Earth's surface. Radiation is a satellite derived product including shortwave (0.2–5 µm) and longwave (5.0–200 µm) downwelling and upwelling radiation at the Earth's surface. The radiation estimates come from the synergistic use of ISCCP cloud dataset, satellite data (TOMS, TOVS and SAGE-II), models (NCEP reanalysis, GISS climate model) and climatologies of various tropospheric and stratospheric parameters (aerosols, water vapour, etc). The dataset spans from July 1983 to December 2009 having a temporal resolution of 3 h and a spatial resolution 280 km × 280 km (~ 2.5° × 2.5°). Zhang et al. (2004) estimated the uncertainty of the dataset at 10–15 W m^{-2} compared with the ERBE (Earth Radiation Budget Experiment) and (Clouds and the Earth's Radiant Energy System) CERES datasets. Since the ISCCP radiation data emerge from the use of a complete radiative transfer model from the GISS global climate model with observations of ISCCP surface, atmosphere and cloud physical properties as input, the radiation and cloud datasets are considered fully compatible. For the current analysis, seasonal averages of the ISCCP variables were calculated for the time period 1990–2008 and were compared to the WRF surface downward short- and longwave radiation, after bilinear interpolation to the 2.5° × 2.5° ISCCP grid.

Model cloudiness was validated against the well established cloud product from ISCCP, obtained from operational sensors aboard geostationary and polar-orbiting satellites (Rossow and Schiffer, 1999). Single pixel observations in the visible (0.6 mm and 1 km resolution) and infrared (11 mm and 1–4 km resolution depending on the instrument) spectral bands are used. Pixels appearing to be colder and/or brighter than clear sky are characterized as cloudy. Pixel-level retrievals are spatially aggregated at

GMDD
7, 6629–6675, 2014

an equal area grid with a resolution of 280 km × 280 km, being available 8 times per day. The ISCCP cloud product is in good agreement to the MODIS cloud mask product (Pincus et al., 2012).

An additional, higher resolution, satellite dataset was also used for model validation, in order to confirm the robustness of the validation findings with ISCCP. Shortwave downward radiation at the surface was additionally obtained from Satellite Application Facilities for Climate Monitoring (CMSAF), which is part of the European Organization for the Exploitation of Meteorological Satellites (EUMETSAT). The spatial resolution of the data is 0.03° × 0.03° while the temporal resolution is 15 min. There is a total of six MFG satellites (Meteosat-2 to 7), providing SSR data from 1983 to 2005. This dataset has been validated against homogenized ground-based observations from the Global Energy Balance Archive (GEBA) (Sanchez-Lorenzo et al., 2013) and from the Baseline Surface Radiation Network (BSRN) (Posselt et al., 2012). In this study, seasonal mean solar surface radiation data from CMSAF were re-gridded to the EOBS 0.44 domain in order to be compared with the WRF simulations for the time period 1990–2005. Since this dataset does not exactly overlap with the hindcast timeslice (1990–2008), we used the higher resolution dataset only as auxiliary material to support the major findings of the model comparison with the coarser ISCCP satellite retrievals.

2.2 Models

In this work we present EURO-CORDEX hindcast climate simulations performed with the WRF/ARW (version 3.3.1) model. The simulations cover the EURO-CORDEX domain with a resolution of 0.44°. Some options are common to all the simulations. The Noah Land Surface Model (NOAH) was the commonly selected land surface model (Chen et al., 1996), the Yonsei University scheme (YSU) was the chosen Planetary Boundary Layer (PBL) scheme (Hong et al., 2006) and MM5 similarity the surface layer option. All simulations were forced by the ERA-interim reanalysis dataset (Dee et al., 2011) at 6 hourly intervals with a spatial resolution of 0.75. The way the forcing fields were pre-processed and implemented in the simulations (relaxation zone, method etc),

GMDD
7, 6629–6675, 2014

the setting of vertical layering, land use databases, or sea surface temperatures were decided by each group separately.

In the current ensemble, five different WRF configurations are applied (Table 1). Three different convection schemes were used, namely the Kain–Fritsch (KF, Kain, 2004), the Grell–Devenyi (GD, Grell and Devenyi, 2002) and the Betts–Miller–Janjic ensemble (BMJ, Janjic, 2000). The radiation physics options tested were: the newer version of the Rapid Radiative Transfer Model (RRTMG, Iacono et al., 2008) and the CAM scheme (Collins et al., 2004). The selected microphysics options were the WRF Single-Moment 3 and 5-class schemes (WSM3/WSM5, Hong et al., 2004) and the WRF Single-Moment 6-class schemes 6 (WSM6, Hong and Lim, 2006). WRF_A configuration is simulated twice with different SSTs (WRF_A and WRF_A_SST). In WRF_A_SST, the SST field was interpolated as provided in the standard 3.3.1 release (METGRID.TBL). This option results in a coarse resolution of the SSTs resulting in a strong temperature perturbation across the European coastline. In other configurations, either a finer interpolation method is used or the SST fields are replaced by skin temperature.

Five meteorological variables are evaluated, namely surface temperature, precipitation, total cloud cover, the short- and longwave downward radiation at the surface. Temperature and precipitation fields were interpolated to the 0.44 E-OBS grid and an elevation correction (standard lapse rate of $6\,^{\circ}\mathrm{C\,km^{-1}}$) was applied to the simulated temperature to account for the difference between EOBS9 and model orography. Radiation and cloud data were bilinearly interpolated to a common ISCCP 2.5° grid for comparison to the satellite dataset.

2.3 Methodology

Mean surface temperature, precipitation and solar radiation were calculated for the time period of interest (1990–2008). One year (1989) was used by all simulations as spin up time. In particular, this spin-up allows for adjustment of the soil moisture and temperature. The seasons were averaged from June to August (JJA) and December

GMDD
7, 6629–6675, 2014

to February (DJF). All seasonal averages were calculated based on mean monthly values. The analysis is undertaken over the whole European domain and over the following sub-regions: Alps (AL), British Isles (BI), East Europe (EA), France (FR), Mid-Europe (ME), Mediterranean (MD), Iberian Peninsula (IP) and Scandinavian Peninsula (SC). These sub-domains are described in Christensen and Christensen (2007).

Taylor diagrams are used to provide a concise statistical summary of how well observed and simulated patterns match each other in terms of their correlation R and normalized standard deviation (NSD) (Taylor, 2001). The correlation (either spatial or temporal) is indicated as the azimuthal position of the point in the 2-D polar coordinate plot and the NSD is represented by the radial distance from the reference point, the latter having R and NSD equal to unity. Points lying close to the reference point are both correct in phasing and amplitude of variation.

Q–Q plots are probability plots comparing two probability distributions by plotting their quantiles against each other. Following the methodology of Garcia-Diez et al. (2013) we compare the distributions of simulated mean temperature and precipitation (y axis) against the observations (x axis). The probability range is divided so that a quantile is taken for every 5 % (19 intervals). The points in the Q–Q plot will approximately lie on the $y = x$ line, if the two distributions are similar. Biases in the model distribution appear in the Q–Q plot as shifts from the $y = x$ line, asymmetries as curved lines and differences in variability as lines with different slopes.

In order to test the statistical significance of differences between models and observations of we calculate the quantity t (two-independent sample t test):

$$t = (X_m - X_o)/\sqrt{\left(\sigma_m^2 + \sigma_o^2\right)/n}$$

where X_m and X_o are the arithmetic means of the $n = 57$ monthly values for one season in the 19 year time slice; σ_m and σ_o are the SDs of the n values. The modelled and observed values are significantly different at the 95 % level if $t > 1.98$.

GMDD
7, 6629–6675, 2014

3 Results

3.1 Surface temperature

3.1.1 Bias

The mean climatological patterns and the annual cycle of temperature are captured quite well by all model configurations, following the spatial characteristics of EOBS9. This supports the view that major processes governing the surface temperature climatology are represented reasonably by all model configurations. Figure 1 shows the summer and winter mean surface 2 m temperature bias with respect to EOBS9 over Europe averaged over the time slice 1990–2008. Stippling indicates areas where the biases are not statistically significant; over all other regions the models and observations are significantly different at the 95 % level. Table 2 summarizes the EOBS9 mean seasonal averages of surface temperature over the different subregions, the absolute model bias (model-EOBS9) of all simulations and the ERA-Interim comparison with EOBS (ERA-Interim minus EOBS9). The forcing fields (ERAi) are somewhat warmer ($\sim 0.5\,^{\circ}$C) over the whole European domain compared to EOBS9 data. Nearly all WRF configurations underestimate surface temperatures over the different European subregions for both seasons. Only the upper quantiles of JJA mean-temperature are overestimated mainly in southern Europe (MD, IP), as indicated by the Q–Q plots (Fig. S1a). Otherwise, the bias remains systematically negative for all configurations, with no obvious asymmetries or differences in variability, except for the behaviour of WRF-G in summer and WRF-A_SST in winter, which are discussed thoroughly in the following sections.

Mooney et al. (2013) in a WRF-multi physics ensemble forced by ERA-Interim, reported that summer surface temperature is mostly controlled by the selection of Land Surface Model (LSMs). In their study the NOAH and Rapid Update Cycle (RUC) LSMs were tested, and the use of NOAH yielded more accurate surface temperatures than the use of RUC, however the temperature distributions were shifted towards lower

GMDD
7, 6629–6675, 2014

values, especially when combined with the CAM radiation scheme. Our current findings can neither support nor contradict this finding, since all models are using the NOAH LSM. We could tentatively attribute, however, the combination of the NOAH LSM along with the CAM radiation scheme, as one possible explanation contributing to the general tendency towards cold biases in the WRF-ensemble.

Of all our WRF simulations, WRF-G has the largest cold bias in summer (−2.1 °C mean over all European sub-regions). WRF-G uses the GD convective scheme, which may explain the larger cold bias, since the other configuration using the same microphysics (WSM6) and radiation (CAM) as WRF-G, with a different convective scheme (WRF-A with KF scheme) has a smaller bias (−0.3 °C). Analysis of the short- and long-wave radiation components further support this finding, as shown below.

In winter a negative temperature bias is apparent for all model configurations especially over the north-eastern part of Europe and as indicated by the winter mean temperature Q–Q plots (Fig. S1b), this underestimation mostly concerns the lower quantiles of the distribution. This finding in not uncommon among different climate simulations including global modelling studies within CMIP5 (e.g. Cattiaux et al., 2013). Mooney et al. (2013) reported that the radiation scheme (especially the long wave component) has a large impact on winter surface temperature, the CAM option being related to greater negative bias over north and east Europe in comparison to RRTMG. Our simulations do support this finding, since WRF-D and WRF-F using the RRTMG radiation scheme exhibit the smallest bias in winter over the EA domain (−0.2 and 0.6 °C respectively). The bias in Scandinavia ranges from −1 to −3 °C in the current ensemble during winter.

Interestingly, the same subregions (SC, EA) apart from exhibiting the largest bias, are also the areas with the highest spread in temperature, as indicated by the SD contours (not shown). Moreover, the differences between the observed and model distributions over this area are statistically significant for all model configurations. Wintertime SDs are considerably larger than summertime and mostly located over north-east Europe (3–4 °C) with a northeast-southwest gradient. This spatial pattern of higher uncertainty

GMDD
7, 6629–6675, 2014

(spread) over north-east Europe has also been reported in future climate projections for winter temperature, and related to the role of snow cover in cooling down the surface through snow albedo and snow emissivity feedbacks (Deque et al., 2007). Another issue for consideration is that the working WRF version has known problems in treating surface temperature in snow covered areas[1]. Garcia-Diez et al. (2014b) show also in their 5 year long multi-physics EURO-CORDEX ensemble that the snow-covered European regions (Alps, and north-east Europe) overestimate the surface albedo, which may be among the sources of bias.

WRF-A_SST has an even colder bias for both seasons in comparison to WRF-A, despite using the same primary parameterizations. This disagreement can be attributed to the SST implementation (coarse resolution along the coastline). This perturbation of SSTs affects considerably the inner part of the domain in winter, by lowering the surface temperature, as indicated by additional 1 year long sensitivity studies with the WRF-A_SST modelling system (results not shown here). In the 19 years hindcast simulations, this effect is not so pronounced in summer. The southern part of the Scandinavian Peninsula, the UK and Italy are the areas with the highest temperature differences in winter. This increases the spread in these areas even more, and thus uncertainty in winter temperature, which has already been shown to be large above north-east Europe in winter.

The causal link between SSTs and land surface temperature is not easy to depict as they both may influence one another and third factors may influence both at the same time. A similar behaviour is also reported by Cattiaux et al. (2011) in a North-Atlantic SST sensitivity experiment of the fall and winter 2006/2007 with a climatic (colder) SST dataset. A similar response in land surface temperature above Europe was showcased, in which anomalous SSTs affected land temperature through the upper-air advection of heat and water vapor, interacting with radiative fluxes over the continent. This mechanism was also found to be more pronounced in autumn and winter, when SSTs anomalies and upper air advection is more efficient.

[1] www.atmos.washington.edu/~cliff/WRFWorkshop2013.ppt

GMDD
7, 6629–6675, 2014

3.1.2 Temporal and spatial agreement

We use Taylor plots (Taylor, 2011) to investigate the temporal agreement between the simulated and observed fields. With area-averaged temperature fields, we compare time-series of spatially averaged quantities. Figure 2 (upper panel) depicts model performance with different colours depicting the different WRF configurations. The overall model performance based on average monthly values, indicates very high temporal agreement with observations (0.95) and amplitude of variability higher than the observational ($\sigma_{norm} > 1$). Inspection of Taylor plots for each different European subregion (not shown), shows that the largest amplitude of variability is produced by WRF-F/WRF-G and the lowest (σ_{norm} slightly below unity) for WRF-C. The worst performance with respect to temporal correlations is found over the Alps for the winter and summer season ($0.7 < R < 0.8$) most probably due to the coarse resolution of the model set up which cannot capture accurately the topographic features of the area.

The spatial agreement between observations and the models is investigated by comparing the time-averaged spatial fields i.e. two maps without a temporally varying component. The spatial agreement over the whole European domain (Fig. 2 bottom) is very high (0.97–0.99), confirming that the spatial representation of surface temperature is captured well. The amplitude of normalized standard deviation (σ_{norm}) in winter is somewhat higher than unity for all configurations. In summer results are more dispersed compared to winter, and the WRF-C configuration again gives the lowest and best (unity) σ_{norm}. On a sub-regional level results appear to have greater spread over over inner continental regions (ME, FR, EA) in comparison to coastal areas (IP, SC, MD, IB) (not shown).

GMDD
7, 6629–6675, 2014

3.2 Precipitation

3.2.1 Bias

All models depict observed climatological features, namely the major precipitation maxima over the Alps (smaller in winter) and western Norway and the dry regions over the Mediterranean in summer (not shown). Precipitation is overestimated for both seasons over all subregions, except for the British Isles in winter (−5 to −15 % relative bias depending on the configuration) (Table 3). The precipitation bias is larger in summer, ranging between 25 to 55 % for the different model configurations, than in winter (15 to 30 %).

Figure 3 shows the mean bias in precipitation for all model configurations. The difference between modelled and observed values is statistically significant for all configurations over most subregions. The models show the largest deviation from observations for summer precipitation magnitudes in the Mediterranean area, especially if the KF convective scheme is selected. Convective precipitation along the Dinaric Alps is overestimated in the WRF-C and WRF-A configurations such that the model precipitation is almost double that of the observations. The issue of unrealistically high summer convective precipitation over mountainous regions is also discussed by Torma et al. (2011) and Zanis et al. (2014), indicating that the bias improves in higher resolution simulations by optimizing the convection scheme. Higher precipitation rates (upper quantiles) are overestimated over all subregions for all model configurations (Fig. S2a). Herwehe et al. (2014) in their study over North America, also reported a large overestimation in larger summertime precipitation amounts (> 2.54 cm), attributed to deep cumulus convection. This large overestimation was improved considerably when subgrid-scale cloud-radiation interaction were introduced into the WRF model into the KF convection scheme (Alapaty et al., 2012).

The lowest summer precipitation bias is noted when the GD convective scheme is used (about 25–30 % on average), followed by the BMJ (about 35 %). The KF scheme is related to the highest positive precipitation bias over all European sub-regions but

GMDD
7, 6629–6675, 2014

the Scandinavian Peninsula (50–55 % in summer and 20–30 % in winter). Results are more comparable in winter: the most problematic area with respect to bias appears to be Eastern Europe (50–65 % for different model options) while for all other European sub-regions the bias is considerably lower (20–30 %).

Precipitation overestimation is not an uncommon feature in WRF simulations (Diez et al., 2014b), and often becomes more pronounced at higher resolutions. This systematic error may reflect an unbalanced hydrological cycle, returning moisture from land and/or water bodies to the atmosphere too quickly. Kotlarski et al. (2014) suggest that the wintertime wet bias of WRF is closely related to the distinct negative bias of mean sea-level pressure, indicating a too high intensity of low pressure systems passing over the continent. However, some sensitivity studies performed at WRF-F using spectral nudging for upper air winds and thereby avoiding this problem, showed little changes in bias amplitude (R. Vautard, personal communication, 2014). Sensitivity tests conducted to test alternative choices for convective parameterizations and cloud microphysics are also usually not conclusive but generally none of the options decisively improve the general picture at higher resolutions (Bullock et al., 2014).

Figure 4 depicts the annual cycles of all model configurations based on mean monthly values, over the selected subregions. The shaded area corresponds to the observational SD. All configurations reproduce reasonably well the basic characteristics of the seasonal cycle, such as the dry summer of southern Europe or the summer maximum over Scandinavia. All simulations have a wet bias, mostly during spring- and summertime and to a lesser extent in autumn and winter. This fact points to smaller-scale circulations and convection being a critical component to the large positive bias in precipitation. Higher correlations of the modeled with observed annual cycles are seen over the Mediterranean, the Iberian and the Scandinavian Peninsulas, despite the large positive bias. Results are more dispersed and less correlated for the Alps and the Mid-European regions. In few cases the models have difficulties to capture correctly the seasonal cycle over France (WRF-C, WRF-G, WRF-F).

GMDD
7, 6629–6675, 2014

The perturbed SSTs in the WRF-A_SST simulation result in a drier climate throughout the year. The physical reason of this colder and drier climate, can be traced on the water holding capacity of the atmosphere limits precipitation amounts in colder conditions, assuming a small change in the average relative humidity. Depending on the energetic constraints of a region and its water limitations this relation is modulated accordingly for each season and subregion (Trenberth and Shea, 2005). It should be noted, that the reduced precipitation in WRF-A_SST simulations improves considerably the precipitation bias (Table 2) to about 15 % on average for both seasons. However, that this is just a case of error compensation, based on the basic WRF feature of predominant overestimation in precipitation.

3.2.2 Temporal and spatial agreement

Following the same methodology described above for temperature, we proceed with the analysis for precipitation. The temporal Taylor plot based on mean monthly values and averaged over all European subregions (Fig. 5, upper panel) for precipitation shows that the average JJA temporal correlation is 0.8 for all configurations, with amplitudes of variability being close to unity for WRF-F/WRF-G (GD convection) and somewhat higher for all other configurations. The impact of the selection of convective scheme is clearly seen in the summer season but not in winter. For DJF precipitation, the metrics improve somewhat in comparison to those during the warm period ($0.8 < R < 0.9$ and $\sigma_{\text{norm}} \sim 1$), therefore it seems that WRF captures better the temporal variability in winter than summer, apart from having a lower wet bias. The temporal correlation over the Alps is the lowest in the sub-regional analysis ($0.3 < R < 0.6$) and larger over the Scandinavian Peninsula (0.9 in winter and 0.6–0.8 in summer).

With respect to precipitation spatial agreement with observations (Fig. 5, bottom), it seems that DJF WRF results are coherent, and that the different model parameterizations do not impact much on the average winter spatial pattern. The average spatial correlation is about 0.7 and the amplitude of variability 1.1 to 1.2. In summer results are more dispersed with spatial correlations ranging from 0.8 to 0.9 and higher amplitudes

GMDD
7, 6629–6675, 2014

of variability (1.2–1.5), indicating that the amplitude of JJA spatial variation is overestimated. This is a common finding among regional climate model studies, reporting summer precipitation to be mostly controlled by internal convection processes, and winter patterns most likely linked to the large scale circulation and thus the forcing fields (e.g. Rauscher et al., 2010). On a subregional level, the highest spatial correlations is seen over the Scandinavian Peninsula and the British Isles ($R = 0.9$) in winter and the worst over France and Mid-Europe in summer ($R = 0.4$). The amplitude of variability is exaggerated by all model configurations in summer ($1.5 < \sigma_{\text{norm}} < 2$), with the exception of the British Isles (σ_{norm} close to unity).

3.3 Radiation

The primary driver of latitudinal and seasonal variations in temperature is the seasonally varying pattern of incident sunlight, and a fundamental driver of the circulation of the atmosphere are the local-to-planetary scale imbalances between the shortwave (SW) and longwave (LW) radiation. The impact of the distribution of insolation on temperature can be strongly modified by the distribution of clouds and surface characteristics. In the current section we evaluate two radiation components of the WRF model simulations, namely the surface downwelling SW and LW, which are compared to available ISCCP satellite measurements. The comparison was also performed with the CMSAF satellite dataset, available in a higher spatial resolution, but only between 1997–2003.

3.3.1 Downward shortwave radiation at the surface

Seasonal average 1990–2008 downward SW radiation components from WRF and ISCCP satellite data are compared over the European domain. Satellite observations exhibit a south-north gradient in summer, with a maximum over the Mediterranean (up to 400 W m^{-2}) and minima over northern Europe (about 200 W m^{-2} on average). All model configurations exhibit this south-north gradient, however with different characteristics:

GMDD
7, 6629–6675, 2014

in some configurations (WRF-A/WRF-C with KF or WRF-D with BMJ convection) the SW radiation gradient is less steep towards the north compared to the satellite data, leading to a general positive SW bias over Europe except Scandinavia with a maximum over central Europe, within the range of 40–60 % (Fig. 6a). For WRF-F and WRF-G (GD convection) the SW radiation decreases very steeply near 40–45°, leading to negative bias of SW radiation over North Europe. This can explain, at least partially, the larger negative temperature bias of summer temperature over mid-Europe and North Europe for WRF-G and WRF-F, compared to other configurations.

Interestingly, Garcia-Diez et al. (2014b) showed that the negative SW radiation bias over central and North Europe in summer in the WRF-G configuration is not reproduced in a 5 year long simulation, when the model simulation restarts daily from the ERA-interim forcing fields with 12 h of spin-up. Thus, it appears this radiation bias is related to internal physical mechanisms, and eventually feedbacks, which develop in a years-long climate simulation. As it will be shown later, the underestimation of SW downward radiation at the surface in GD convection can be linked to a 40–50 % overestimation of cloudiness.

In winter the observational data indicate maxima of the SW radiation values of about 160 W m^{-2} over the southern part of the domain that decreases gradually towards the north. The same spatial pattern is reproduced by all model configurations; however, there is mostly a positive SW radiation bias over the domain, except the Iberian Peninsula and north European coasts of France and Benelux (Fig. 6b). The positive bias increases towards the north and east parts of the domain, where it reaches up to 70–80 %. WRF-C, with different microphysics (WSM3) has an additional feature, exhibiting higher positive SW radiation bias over Mid- and East-Europe (~ 70 %).

3.3.2 Downward longwave radiation at the surface

Downward LW radiation in summer is higher over southern Europe and decreases towards the north. Comparison with the ISCCP satellite data indicates a negative bias over southern Europe of about 20 % – more pronounced for the KF convective scheme

GMDD
7, 6629–6675, 2014

– becoming positive in northern Europe with larger positive bias with the GD convective scheme (10 %) (Fig. 7a). Comparison of Figs. 6a and 7a (SW and LW components) shows that summer SW and LW biases are generally anti-correlated, in such a way that regions with positive SW bias, exhibit a negative LW bias and vice versa. If the magnitude of biases were the same, then there would be a cancelling in radiation bias and a better agreement with observed temperature would be expected. However, this is not the case.

For WRF-A and WRF-C configurations using the KF convection and CAM radiation schemes there is a strong surplus in downward radiation (SWbias + LWbias > 0) over central and southern Europe, leading to lower cold bias or even small warm biases in southern Europe in comparison to northern Europe (Fig. S3a).The BMJ/RRTMG configuration (WRF-D) has the same features with more enhanced and extended radiative balance surplus extended in east Europe. The GD/CAM (WRF-G) configuration has a predominant summer negative SW radiation bias in north Europe, a smaller in magnitude and positive bias in LW, resulting in a deficit downward radiation regime (SWbias + LWbias < 0). Over south Europe the signs change (positive SW bias/small negative LW bias) resulting in a surplus downward radiation regime (SWbias + LWbias > 0). This feature explains the pronounced cold bias in north Europe which becomes lower while moving southwards.

The winter LW climatology (not shown) correlates well spatially with the temperature patterns. It is minimized over north-east Europe and increases towards the south- and western parts of Europe. The winter LW bias is for all model configurations negative over almost all Europe (Fig. 7b), only smaller or even positive along the north-west European coast (France, Benelux, Denmark, Baltic countries), compensating for the SW radiation surplus discussed previously. Since the SW amounts over north European winter are very small, the radiation regime is regulated by the LW radiation component, exhibiting a deficit (SWbias + LWbias < 0) over north and north-east Europe, which decreases or even becomes positive (WRF-G/WRF-F) in south and south west Europe (Fig. S3b).

GMDD
7, 6629–6675, 2014

3.3.3 Total cloud cover

Since cloudiness is a key component in the discussion concerning radiation, we compare our model results with total cloud cover (CC) of the ISCCP satellite retrievals. During the summer season, observations indicate increased CC over the north and west part of the domain (CC > 0.8) i.e. the north-east Atlantic, and the lowest CC in southern Europe (lat < 40°). All WRF configurations have a similar pattern, underestimating CC in southern Europe (Fig. 8a), by more than 50 %. The GD configurations with the GD convective scheme have an additional positive bias over northeast Europe. This pattern is very well correlated with the SW radiation bias discussed above, indicating that cloudiness and SW radiation biases have opposite signs, as expected. Herwehe et al. (2014) in a climatic application of WRF over North America reported also an underestimation of summertime cloud fraction over the south-eastern part of their domain, which was considerably improved in their modified case including the sub-grid scale correction in the KF convection scheme. The most pronounced improvement was found in the middle cloud layer (700–500 hPa) consistent with the deep convection of summer. The addition of sub-grid scale cloudiness in the modified case had also the anticipated effect of decreasing in the SW downwelling radiation at the surface and a better agreement with satellite data. The impact on the LW radiation component was minor.

In winter the observed CC has a more pronounced peak over the north-west part of the domain over the sea, and reduces gradually towards the south with a secondary maximum over the Black Sea and minima over the Iberian Peninsula (not shown). The bias pattern in winter (Fig. 8b) is negative over the Mediterranean (−20 to −30 %) (except in configurations with the GD convective scheme) and positive over north and north-east parts of Europe (40 to 50 %). The higher than observed modeled cloudiness over northern Europe eventually reduces the amounts of SW radiation reaching the surface, but the positive SW bias remains. Note however, that winter SW radiation absolute amounts are very small over north Europe in winter, so that large relative

GMDD
7, 6629–6675, 2014

biases (60–70 %) over this area correspond to small absolute changes, which lie within the uncertainty of the satellite data (Zhang et al., 2004).

The wintertime positive bias of cloud cover over north Europe is accompanied by negative bias in the LW downward radiation at the surface, in all model configurations. There is not a straightforward explanation for this feature, since increased cloudiness should be associated with increased LW radiation. Both model and observational datasets are internally consistent (the cloud and radiation components), since the ISCCP radiation data are derived by the cloud data (see Sect. 2.1), while WRF has its own internally consistent physics. The results are robust, since they are reproduced by Garcia-Diez et al. (2014b) in their 5 year simulations of the same ensemble, validated with a different satellite dataset.

In order to provide answers several issues should be investigated, including a more detailed analysis of cloud coverage and the various radiation components i.e. what are the type of clouds and their impact on the radiation budget. It is well known that low clouds are thick and non-transparent, reflecting too much of SW radiation back to space (high cloud albedo forcing) and – having almost the same temperature as the surface – do not greatly affect the LW radiation. On the other hand, high thin cirrus clouds are highly transparent to SW radiation but they readily absorb LW radiation. Since they are high and therefore cold, they have a large cloud greenhouse forcing. Finally, the deep convective clouds have a neutral effect since the cloud greenhouse and albedo forcings almost balance. It is clear from the current study, that further analysis is necessary, including short- and longwave radiation components, both at the surface and at the top of the atmosphere, as well as various cloud properties which are derived by satellites and are available as output variables in WRF (altitude, optical thickness, cloud albedo).

4 Conclusions

Analysis of the WRF ensemble within the EURO-CORDEX framework indicates that the model can represent the present climate with a reasonable degree of fidelity.

GMDD
7, 6629–6675, 2014

Temperatures are on average underestimated and the largest temperature spread and bias is seen in winter over north east Europe. Precipitation is overestimated in both seasons but mostly in summer. These general conclusions apply to all ensemble members, the biases range depending on the model configuration and the physical parameterizations selected.

Summer temperatures are characterized by a cold bias, more pronounced in north Europe for the CAM radiation scheme, and less pronounced, or even slight warm bias for south Europe for the RRTMG radiation scheme. The coldest temperature bias in north Europe is related to an underestimation of SW radiation at the surface and an overestimation of cloud cover, mostly seen in configurations using the GD convective scheme. The strong positive SW bias is summer in southern Europe, mostly induced by the KF or BMJ convective schemes, contributes to a lessening of the systematic cold bias of WRF. When a convective scheme does not suffer from a positive SW bias, then temperatures are grossly underestimated (in our case WRF-G configuration with GD convection).

Winter surface temperatures are affected in snow covered areas in north-east Europe, as a result of a too-strong response of temperature to snow cover. The negative sign in the sum of LW+SW bias over north Europe, contributes to the cold bias problem of the region. Winter cold bias reduces with the application of RRTMG vs. the CAM radiation scheme. Mind also, that ERA-Interim has a small (0.4 °C) positive bias in comparison to our reference EOBS9 climatology. If the driving fields suffer from persistent cold bias they can deteriorate even further model performance even further.

Precipitation overestimation is reported as a typical WRF behaviour, which remains or even worsens in higher spatial resolutions (Kotlarski et al., 2014). Our current findings are in the same line, with the KF convective scheme being related to the highest bias over the Mediterranean in summer. All ensemble members better capture winter than summer precipitation, the latter being locally rather than large-scale controlled. There is no specific configuration that totally alleviates the wet bias of WRF both here and according to literature. This issue points, among other things, towards

GMDD
7, 6629–6675, 2014

weaknesses of convective schemes. The precipitation spread of the EURO-CORDEX WRF-ensemble analyzed by Garcia-Diez (2014a), could only be partially attributed to the selected physical parameterizations. Different model domain configurations and datasets seemingly contribute to the precipitation spread. Our study identifies the implementation of SSTs as one important contributing factor. Erroneously, a coarser resolution of implemented SSTs (WRF-A_SST) seemingly "corrects" the average WRF wet bias, by shifting the average climatology towards a colder-drier winter climate regime.

Concluding, we stress the importance of such coordinated evaluation exercises, which aim to highlight systematic bias in model performance, and identify the underlying physical mechanisms. The current work evaluates only the surface components of the radiation balance without those at the top of the atmosphere, the sensible and latent heat fluxes or looking into cloud properties. Future analyses including these parameters is necessary for a more thorough interpretation of the physical mechanisms involved in the appearance of temperature and precipitation biases. This work is ongoing within the EURO-CORDEX WRF-groups.

The Supplement related to this article is available online at doi:10.5194/gmdd-7-6629-2014-supplement.

Acknowledgements. We acknowledge the E-OBS dataset from the EU-FP6 project ENSEMBLES (http://ensembles-eu.metoffice.com) and the data providers in the ECA&D project (http://www.ecad.eu).

Aristotle University of Thessaloniki simulations have been produced using the EGI and HellasGrid infrastructures and supported by the Scientific Computing Center at the Aristotle University of Thessaloniki. Katragkou E. acknowledges financial support from the AUTH-Special Account for Research Funds.

The contribution from Centre de Recherche Public – Gabriel Lippmann was funded by the Luxemburg National Research Fund through the Grant FNR C09/SR/16 (CLIMPACT).

Alexandri G. and Zanis P. acknowledge financial support from the QUADIEEMS project which is co-financed by the European Social Fund (ESF) and national resources under the operational

GMDD

7, 6629–6675, 2014

programme Education and Lifelong Learning (EdLL) within the framework of the Action "Supporting Postdoctoral Researchers".

The contribution from Universidad de Cantabria was funded by the Spanish R&D programme through projects CORWES (CGL2010-22158-C02-01) and WRF4G (CGL2011-28864), co-funded by the European Regional Development Fund. García-Díez M. acknowledges financial support from the EXTREMBLES (CGL2010-21869) project.

References

Alapaty, K., Herwehe, J. A., Otte, T. L., Nolte, C. G., Bullock, O. R., Mallard, M. S., Kain, J. S., and Dudhia, J.: Introducing subgrid-scale cloud feedbacks to radiation for regional meteorological and climate modeling, Geophys. Res. Lett., 39, L24808, doi:10.1029/2012GL054031, 2012.

Boberg, F. and Christensen, J. H.: Overestimation of Mediterranean summer temperature projections due to model deficiencies, Nat. Clim. Chang., 2, 433–436, doi:10.1038/nclimate1454, 2012.

Bullock, O. R., Alapaty, K., Herwehe, J. A., Mallard, M. S., Otte, T. L., Gilliam, R. C., and Nolte, C. G.: An observation-based investigation of nudging in WRF for downscaling surface climate information to 12-km grid spacing, J. Appl. Meteorol.Clim., 53, 20–33, doi:10.1175/JAMC-D-13-030.1, 2014.

Cardoso, R. M., Soares, P. M. M., Miranda, P. M. A., and Belo-Pereira, M.: WRF high resolution simulation of Iberian mean and extreme precipitation climate, Int. J. Climatol., 33, 2591–2608, doi:10.1002/joc.3616, 2013.

Cattiaux, J., Vautard, R., and Yiou, P.: North-Atlantic SST amplified recent wintertime European land temperature extremes and trends, Clim. Dynam., 36, 2113–2128, doi:10.1007/s00382-010-0869-0, 2010.

Cattiaux, J., Douville, H., Ribes, A., Chauvin, F., and Plante, C.: Towards a better understanding of changes in wintertime cold extremes over Europe: a pilot study with CNRM and IPSL atmospheric models, Clim. Dynam., 40, 2433–2445, doi:10.1007/s00382-012-1436-7, 2012.

Chen, F., Mitchell, K., Schaake, J., Xue, Y., Pan, H.-L., Koren, V., Duan, Q. Y., Ek, M., and Betts, A.: Modeling of land surface evaporation by four schemes and comparison with FIFE observations, J. Geophys. Res., 101, 7251, doi:10.1029/95JD02165, 1996.

GMDD

7, 6629–6675, 2014

Christensen, J. H. and Christensen, O. B.: A summary of the PRUDENCE model projections of changes in European climate by the end of this century, Climatic Change, 81, 7–30, doi:10.1007/s10584-006-9210-7, 2007.

Collins, W. D., Rasch, P. J., Boville, B. A., Hack, J. J., McCaa, J. R., Williamson, D. L., Kiehl, J. T., and Briegleb, B.: Description of the NCAR Community Atmosphere Model (CAM 3.0) NCAR Technical Note, NCAR/TN-464+ST R, available at: http://hanson.geog.udel.edu/~hanson/hanson/CLD_GCM_Experiment_S11_files/description.png (last access: 14 August 2014), 2004.

Dee, D. P., Uppala, S. M., Simmons, A. J., Berrisford, P., Poli, P., Kobayashi, S., Andrae, U., Balmaseda, M. A., Balsamo, G., Bauer, P., Bechtold, P., Beljaars, A. C. M., van de Berg, L., Bidlot, J., Bormann, N., Delsol, C., Dragani, R., Fuentes, M., Geer, A. J., Haimberger, L., Healy, S. B., Hersbach, H., Hólm, E. V, Isaksen, L., Kållberg, P., Köhler, M., Matricardi, M., McNally, A. P., Monge-Sanz, B. M., Morcrette, J.-J., Park, B.-K., Peubey, C., de Rosnay, P., Tavolato, C., Thépaut, J.-N., and Vitart, F.: The ERA-Interim reanalysis: configuration and performance of the data assimilation system, Q. J. Roy. Meteor. Soc., 137, 553–597, doi:10.1002/qj.828, 2011.

Déqué, M., Rowell, D. P., Lüthi, D., Giorgi, F., Christensen, J. H., Rockel, B., Jacob, D., Kjellström, E., Castro, M., and Hurk, B.: An intercomparison of regional climate simulations for Europe: assessing uncertainties in model projections, Climatic Change, 81, 53–70, doi:10.1007/s10584-006-9228-x, 2007.

Flato, G., Marotzke, J., Abiodun, B., Braconnot, P., Chou, S.., Collins, W., Cox, P., Driouech, F., Emori, S., Eyring, V., Forest, C., Glecker, P., Guilyardi, E., Jacob, C., Kattsov, V., Reason, C., and Rummukainen, M.: Evaluation of climate models, in: Climate Change 2013: The Physical Science Basis. Contribution of Working Group I to the Fifth Assessment Report of the Intergovernmental Panel on Climate Change, Cambridge University Press, Cambridge, UK and New York, NY, USA, 2013.

García-Díez, M., Fernández, J., Vautard, R., Gobiet, A., Goergen, K., Güttler, I., Halenka, T., Katragkou, E., Kotlarski, S., Krüzselyi, I., Soares, P., Sobolowski, S., and Teichmann, C.: Multiphysics vs. multimodel spread in the new EURO-CORDEX RCM ensemble, J. Climate, in review, 2014a.

Garcia-Diez, M., Fernandez, J., and Vautard, R.: An RCM multi-physics ensemble over Europe: multi-variable evaluation to avoid error compensation, Clim. Dynam., in review, 2014b.

GMDD
7, 6629–6675, 2014

Giorgi, F., Jones, C., and Asrar, G. R.: Addressing climate information needs at the regional level?: the CORDEX framework, WMO Bulletin, 58, 175–183, 2009.
Giorgi, F., Coppola, E., Solmon, F., Mariotti, L., Sylla, M., Bi, X., Elguindi, N., Diro, G., Nair, V., Giuliani, G., Turuncoglu, U., Cozzini, S., Güttler, I., O'Brien, T., Tawfik, A., Shalaby, A., Zakey, A., Steiner, A., Stordal, F., Sloan, L., and Brankovic, C.: RegCM4: model description and preliminary tests over multiple CORDEX domains, Clim. Res., 52, 7–29, doi:10.3354/cr01018, 2012.
Grell, G. A. and Dévényi, D.: A generalized approach to parameterizing convection combining ensemble and data assimilation techniques, Geophys. Res. Lett., 29, 34–38, doi:10.1029/2002GL015311, 2002.
Hall, A. and Qu, X.: Using the current seasonal cycle to constrain snow albedo feedback in future climate change, Geophys. Res. Lett., 33, L03502, doi:10.1029/2005GL025127, 2006.
Haylock, M. R., Hofstra, N., Klein Tank, A. M. G., Klok, E. J., Jones, P. D., and New, M.: A European daily high-resolution gridded data set of surface temperature and precipitation for 1950–2006, J. Geophys. Res., 113, D20119, doi:10.1029/2008JD010201, 2008.
Herwehe, J. A., Alapaty, K., Spero, T. L., and Nolte, C. G.: Increasing the credibility of regional climate simulations by introducing subgrid-scale cloud-radiation interactions, J. Geophys. Res., 119, 5317–5330, 2014.
Hong, S. and Lim, J.: The WRF single-moment 6-class microphysics scheme (WSM6), J. Korean Meteor. Soc., available at: http://www.mmm.ucar.edu/wrf/users/docs/WSM6-hong_and_lim_JKMS.png (last access: 14 August 2014), 2006.
Hong, S.-Y., Dudhia, J., and Chen, S.-H.: A revised approach to ice microphysical processes for the bulk parameterization of clouds and precipitation, Mon. Weather Rev., 132, 103–120, doi:10.1175/1520-0493(2004)132<0103:ARATIM>2.0.CO;2, 2004.
Hong, S.-Y., Noh, Y., and Dudhia, J.: A new vertical diffusion package with an explicit treatment of entrainment processes, Mon. Weather Rev., 134, 2318–2341, doi:10.1175/MWR3199.1, 2006.
Iacono, M. J., Delamere, J. S., Mlawer, E. J., Shephard, M. W., Clough, S. A., and Collins, W. D.: Radiative forcing by long-lived greenhouse gases: calculations with the AER radiative transfer models, J. Geophys. Res., 113, D13103, doi:10.1029/2008JD009944, 2008.
Jacob, D., Petersen, J., Eggert, B., Alias, A., Christensen, O. B., Bouwer, L. M., Braun, A., Colette, A., Déqué, M., Georgievski, G., Georgopoulou, E., Gobiet, A., Menut, L., Nikulin, G., Haensler, A., Hempelmann, N., Jones, C., Keuler, K., Kovats, S., Kröner, N., Kotlarski, S.,

GMDD
7, 6629–6675, 2014

Kriegsmann, A., Martin, E., Meijgaard, E., Moseley, C., Pfeifer, S., Preuschmann, S., Radermacher, C., Radtke, K., Rechid, D., Rounsevell, M., Samuelsson, P., Somot, S., Soussana, J.-F., Teichmann, C., Valentini, R., Vautard, R., Weber, B., and Yiou, P.: EURO-CORDEX: new high-resolution climate change projections for European impact research, Reg. Environ. Change, 14, 563–578, doi:10.1007/s10113-013-0499-2, 2013.

Janjic, Z.: Comments on "Development and Evaluation of a Convection Scheme for Use in Climate Models", J. Atmos. Sci., 57, 3686–3686, 2000.

Kain, J. S.: The Kain–Fritsch convective parameterization: an update, J. Appl. Meteorol., 43, 170–181, doi:10.1175/1520-0450(2004)043<0170:TKCPAU>2.0.CO;2, 2004.

Kotlarski, S., Keuler, K., Christensen, O. B., Colette, A., Déqué, M., Gobiet, A., Goergen, K., Jacob, D., Lüthi, D., van Meijgaard, E., Nikulin, G., Schär, C., Teichmann, C., Vautard, R., Warrach-Sagi, K., and Wulfmeyer, V.: Regional climate modeling on European scales: a joint standard evaluation of the EURO-CORDEX RCM ensemble, Geosci. Model Dev., 7, 1297–1333, doi:10.5194/gmd-7-1297-2014, 2014.

Pincus, R., Platnick, S., Ackerman, S. A., Hemler, R. S., and Patrick Hofmann, R. J.: Reconciling simulated and observed views of clouds: MODIS, ISCCP, and the limits of instrument simulators, J. Climate, 25, 4699–4720, doi:10.1175/JCLI-D-11-00267.1, 2012.

Posselt, R., Mueller, R. W., Stöckli, R., and Trentmann, J.: Remote sensing of solar surface radiation for climate monitoring – the CM-SAF retrieval in international comparison, Remote Sens. Environ., 118, 186–198, doi:10.1016/j.rse.2011.11.016, 2012.

Rauscher, S. A., Coppola, E., Piani, C., and Giorgi, F.: Resolution effects on regional climate model simulations of seasonal precipitation over Europe, Clim. Dynam., 35, 685–711, doi:10.1007/s00382-009-0607-7, 2009.

Rossow, W. B. and Schiffer, R. A.: Advances in understanding clouds from ISCCP, B. Am. Meteorol. Soc., 80, 2261–2287, doi:10.1175/1520-0477(1999)080<2261:AIUCFI>2.0.CO;2, 1999.

Rummukainen, M.: State-of-the-art with regional climate models, Wiley Interdiscip. Rev. Clim. Chang., 1, 82–96, doi:10.1002/wcc.8, 2010.

Sanchez-Lorenzo, A., Wild, M., and Trentmann, J.: Validation and stability assessment of the monthly mean CM SAF surface solar radiation dataset over Europe against a homogenized surface dataset (1983–2005), Remote Sens. Environ., 134, 355–366, doi:10.1016/j.rse.2013.03.012, 2013.

GMDD
7, 6629–6675, 2014

Skamarock, W. C., Klemp, J. B., Dudhia, J., Gill, D. O., Barker, D. M., Duda, M. G., Huang, X.-Y., Wang, W., and Powers, J. G.: A description of the advanced research WRF version 3, available at: http://oai.dtic.mil/oai/oai?verb=getRecord&metadataPrefix=html&identifier=ADA487419 (last access: 14 August 2014), 2008.

Skliris, N., Sofianos, S., Gkanasos, A., Mantziafou, A., Vervatis, V., Axaopoulos, P., and Lascaratos, A.: Decadal scale variability of sea surface temperature in the Mediterranean Sea in relation to atmospheric variability, Ocean Dynam., 62, 13–30, doi:10.1007/s10236-011-0493-5, 2011.

Soares, P. M. M., Cardoso, R. M., Miranda, P. M. A., Medeiros, J., Belo-Pereira, M., and Espirito-Santo, F.: WRF high resolution dynamical downscaling of ERA-Interim for Portugal, Clim. Dynam., 39, 2497–2522, doi:10.1007/s00382-012-1315-2, 2012.

Stegehuis, A. I., Teuling, A. J., Ciais, P., Vautard, R., and Jung, M.: Future European temperature change uncertainties reduced by using land heat flux observations, Geophys. Res. Lett., 40, 2242–2245, doi:10.1002/grl.50404, 2013.

Taylor, K. E.: Summarizing multiple aspects of model performance in a single diagram, J. Geophys. Res., 106, D07183, doi:10.1029/2000JD900719, 2001.

Torma, C., Coppola, E., Giorgi, F., Bartholy, J., and Pongrácz, R.: Validation of a high-resolution version of the regional climate model RegCM3 over the Carpathian basin, J. Hydrometeorol., 12, 84–100, doi:10.1175/2010JHM1234.1, 2011.

van den Besselaar, E. J. M., Haylock, M. R., van der Schrier, G., and Klein Tank, A. M. G.: A European daily high-resolution observational gridded data set of sea level pressure, J. Geophys. Res., 116, D11110, doi:10.1029/2010JD015468, 2011.

Van der Linder, P.: ENSEMBLES: Climate Change and its Impacts: Summary of Research and Results from the ENSEMBLES Project, Exeter, 2009.

Vautard, R., Gobiet, A., Jacob, D., Belda, M., Colette, A., Déqué, M., Fernández, J., García-Díez, M., Goergen, K., Güttler, I., Halenka, T., Karacostas, T., Katragkou, E., Keuler, K., Kotlarski, S., Mayer, S., Meijgaard, E., Nikulin, G., Patarčić, M., Scinocca, J., Sobolowski, S., Suklitsch, M., Teichmann, C., Warrach-Sagi, K., Wulfmeyer, V., and Yiou, P.: The simulation of European heat waves from an ensemble of regional climate models within the EURO-CORDEX project, Clim. Dynam., 41, 2555–2575, doi:10.1007/s00382-013-1714-z, 2013.

Warrach-Sagi, K., Schwitalla, T., Wulfmeyer, V., and Bauer, H.-S.: Evaluation of a climate simulation in Europe based on the WRF–NOAH model system: precipitation in Germany, Clim. Dynam., 41, 755–774, doi:10.1007/s00382-013-1727-7, 2013.

GMDD
7, 6629–6675, 2014

Zanis, P., Katragkou, E., Ntogras, C., Marougianni, G., Tsikerdekis, A., Feidas, H., Anadranistakis, E., and Melas, D.: A transient high resolution regional climate simulation for Greece for the period 1960–2100: Evaluation and future projections, Clim. Res., in review, 2014.

Zhang, Y., Rossow, W. B., Lacis, A. A., Oinas, V., and Mishchenko, M. I.: Calculation of radiative fluxes from the surface to top of atmosphere based on ISCCP and other global data sets: refinements of the radiative transfer model and the input data, J. Geophys. Res., 109, D19105, doi:10.1029/2003JD004457, 2004.

GMDD

7, 6629–6675, 2014

Table 1. WRF configurations participating in the study.

Label	Institute	Nz/TOA	Microphys.	Cum.	Rad.
WRF-A	CRPGL	50/20 hPa	WSM6	KF	CAM3
WRF-A_SST	AUTH	30/50 hPa	WSM6	KF	CAM3
WRF-C	BCCR	30 m/50 hPa	WSM3	KF	CAM3
WRF-D	IDL	40/50 hPa	WSM6	BMJ	RRTMG
WRF-F	IPSL	32/50 hPa	WSM5	GD	RRTMG
WRF-G	UCAN	30 m/50 hPa	WSM6	GD	CAM3

GMDD
7, 6629–6675, 2014

Table 2a. Means (M_{obs}) of summer (JJA) surface temperature for observations (EOBS9) over 1990–2008 and the European subregions and model mean seasonal bias ($M_{mod} - M_{obs}$). Unit is degree Celsius.

	EOBS9	WRF-A _SST	WRF-C	WRF-A	WRF-D	WRF-F	WRF-G	ERAi
AL	17.1	−1.0	−1.4	−0.4	−0.2	−0.9	−2.1	0.7
BI	14.7	−2.3	−1.2	−0.9	−0.6	−1.2	−2.4	0.3
EA	18.8	−0.1	−0.1	0.3	0.5	−0.1	−2.3	0.4
FR	18.8	−2.1	−1.6	−0.9	−0.3	−1.2	−2.9	0.2
IP	21.8	−0.5	−1.5	0.0	0.9	0.3	−1.0	0.3
MD	21.9	−0.4	−1.1	0.0	0.7	0.5	−1.0	0.9
ME	17.5	−1.6	−0.7	−0.3	−0.2	−1.1	−2.8	0.3
SC	13.6	−2.3	−0.7	−0.5	−0.4	−0.6	−2.6	0.6

GMDD
7, 6629–6675, 2014

Table 2b. Same as Table 2a for winter.

	EOBS9	WRF-A _SST	WRF-C	WRF-A	WRF-D	WRF-F	WRF-G	ERAi
AL	0.5	−3.6	−1.1	−0.3	−0.4	0.3	−0.7	0.0
BI	4.6	−3.2	−0.1	−0.1	0.2	0.7	0.1	0.7
EA	−1.1	−5.2	−2.0	−1.3	−0.2	0.6	−1.9	0.2
FR	5.1	−3.1	−0.5	−0.4	0.0	0.7	−0.6	0.1
IP	7.0	−2.0	−0.9	−0.4	−0.1	0.4	−0.7	0.3
MD	5.0	−5.5	−1.1	−1.0	−0.5	−0.1	−0.9	0.6
ME	1.8	−3.8	−0.9	−0.5	0.2	0.7	−1.0	0.2
SC	−5.3	−7.0	−2.8	−1.8	−1.8	−0.9	−2.2	0.4

GMDD
7, 6629–6675, 2014

Table 3a. Mean (M_{obs}) of summer (JJA) precipitation for observations (EOBS9) over 1990–2008 and the European subregions. Units of EOBS9 in mm day^{-1}. Model relative bias (%).

	EOBS9	WRF-A_SST	WRF-C	WRF-A	WRF-D	WRF-F	WRF-G
AL	3.20	8 %	37 %	28 %	24 %	14 %	21 %
BI	2.45	15 %	34 %	23 %	27 %	−1 %	6 %
EA	2.22	23 %	41 %	49 %	39 %	36 %	33 %
FR	1.75	15 %	83 %	47 %	16 %	37 %	35 %
IP	0.67	−6 %	63 %	63 %	25 %	31 %	15 %
MD	0.83	−1 %	102 %	94 %	64 %	40 %	59 %
ME	2.35	27 %	46 %	42 %	34 %	34 %	23 %
SC	2.46	26 %	33 %	39 %	54 %	22 %	7 %

GMDD
7, 6629–6675, 2014

Table 3b. Same as Table 3a for winter.

	EOBS9	WRF-A_SST	WRF-C	WRF-A	WRF-D	WRF-F	WRF-G
AL	2.53	16 %	14 %	26 %	41 %	17 %	7 %
BI	3.63	−11 %	−4 %	−4 %	−13 %	−11 %	−5 %
EA	1.13	44 %	51 %	65 %	59 %	60 %	65 %
FR	2.15	45 %	33 %	38 %	20 %	18 %	24 %
IP	1.94	7 %	10 %	11 %	−4 %	−15 %	−9 %
MD	1.98	−15 %	33 %	32 %	14 %	1 %	10 %
ME	1.92	42 %	23 %	38 %	28 %	30 %	31 %
SC	2.01	4 %	14 %	24 %	27 %	22 %	21 %

GMDD
7, 6629–6675, 2014

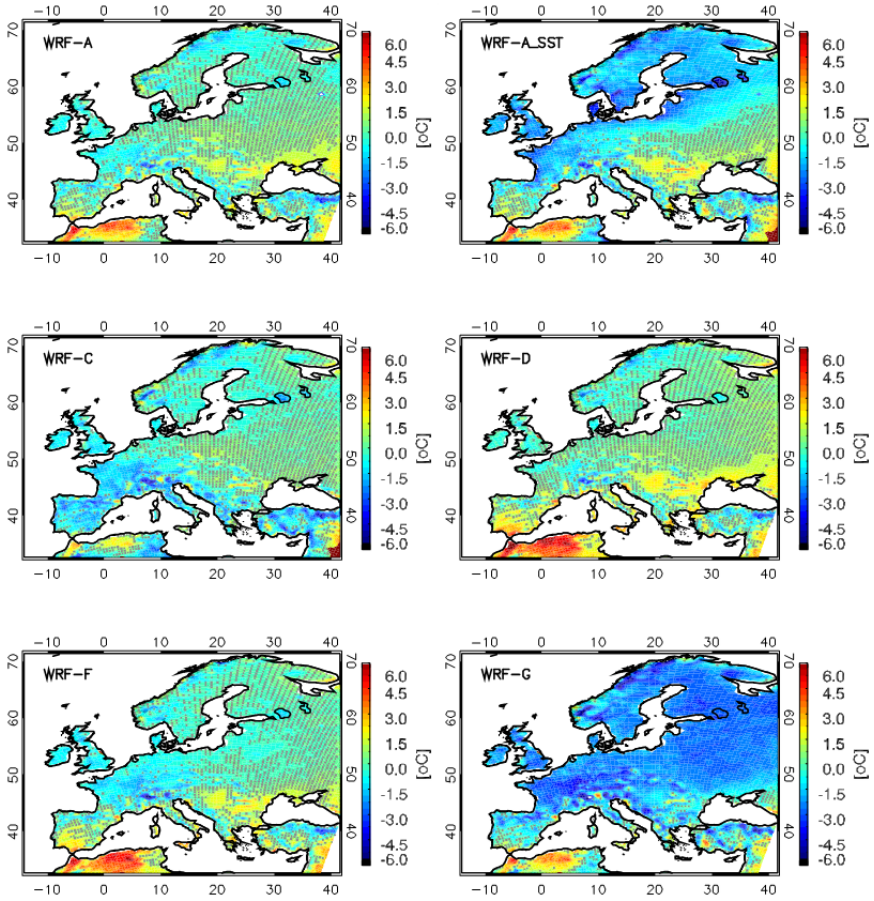

Figure 1a. Mean summer 1990–2008 surface temperature bias (model-EOBS9). Stippling indicates areas where the biases are not statistically significant.

GMDD
7, 6629–6675, 2014

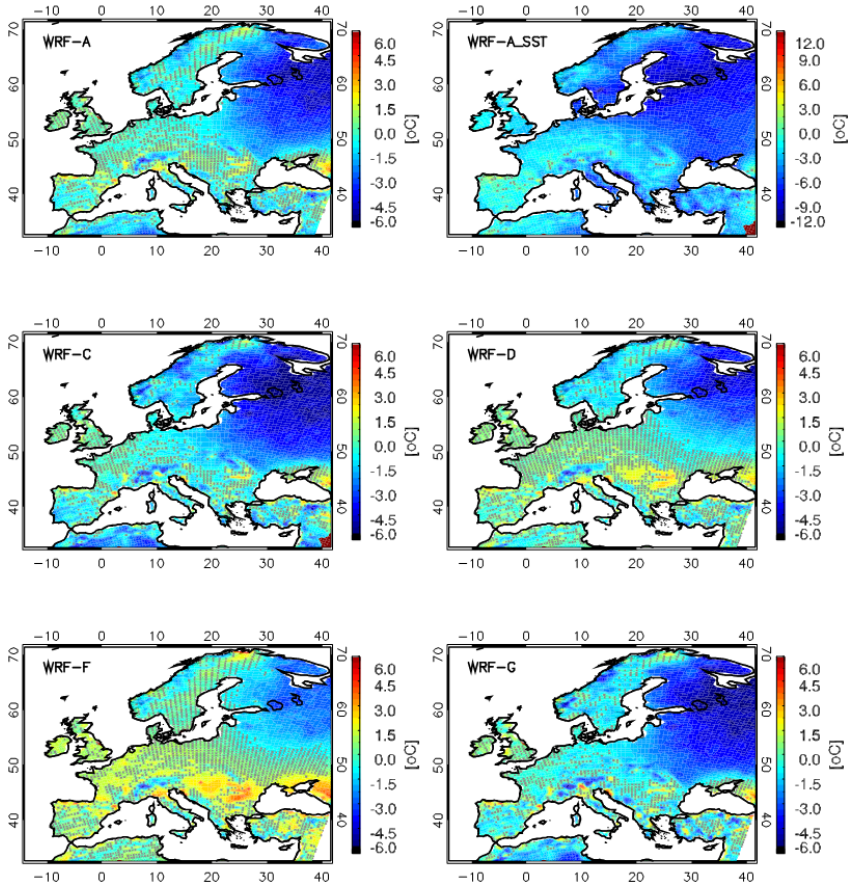

Figure 1b. Mean winter 1990–2008 surface temperature bias (model-EOBS9). Stippling indicates areas where the biases are not statistically significant. Mind the differences in colour scales.

GMDD
7, 6629–6675, 2014

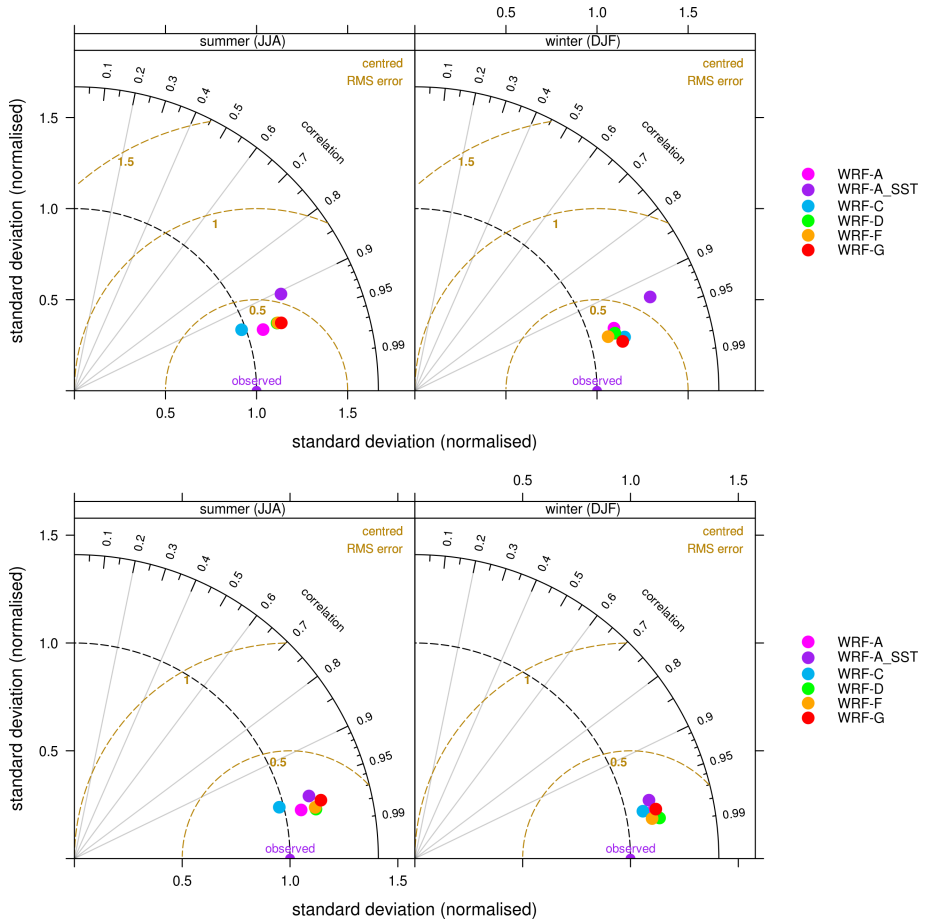

Figure 2. Temporal (upper panel) and spatial (bottom panel) Taylor plots for surface temperature averaged over Europe for summer and winter 1990–2008.

GMDD
7, 6629–6675, 2014

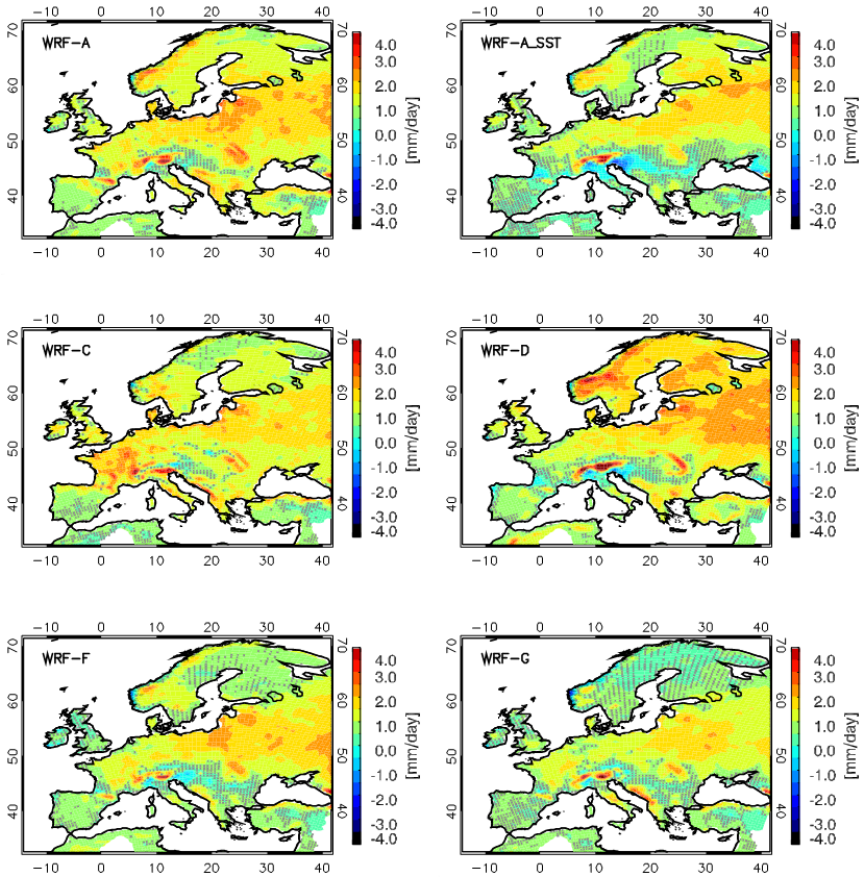

Figure 3a. Mean summer 1990–2008 precipitation bias (model-EOBS9) expressed in mm day^{-1}. Stippling indicates areas where the biases are not statistically significant.

GMDD
7, 6629–6675, 2014

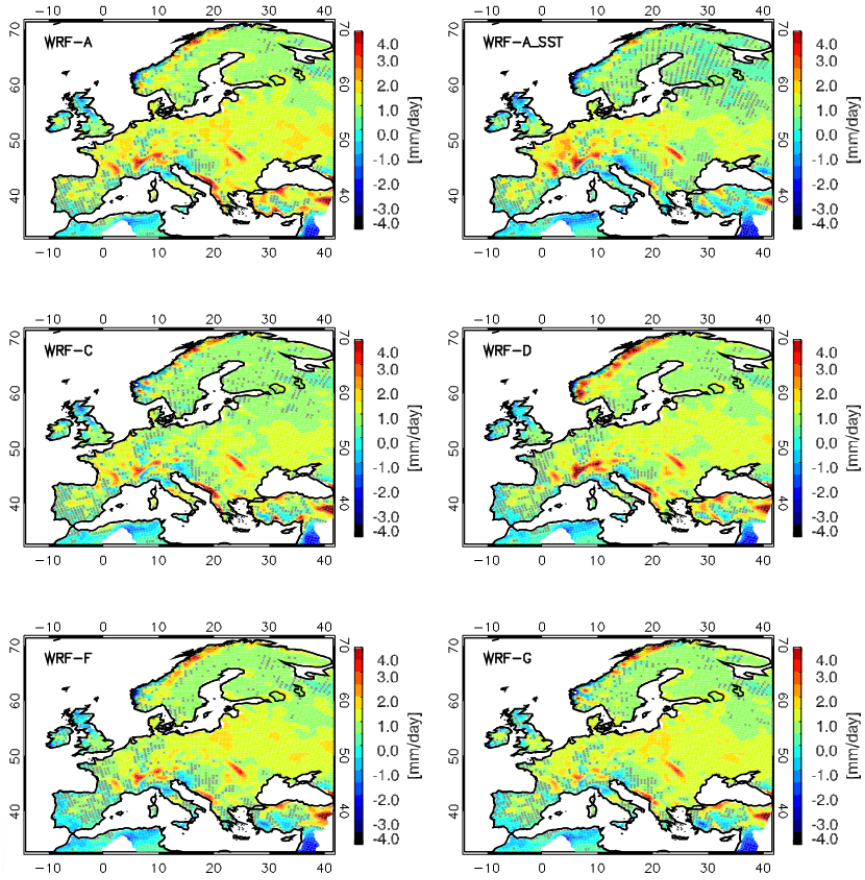

Figure 3b. Mean winter 1990–2008 precipitation bias (model-EOBS9) expressed in mm day^{-1}. Stippling indicates areas where the biases are not statistically significant.

GMDD
7, 6629–6675, 2014

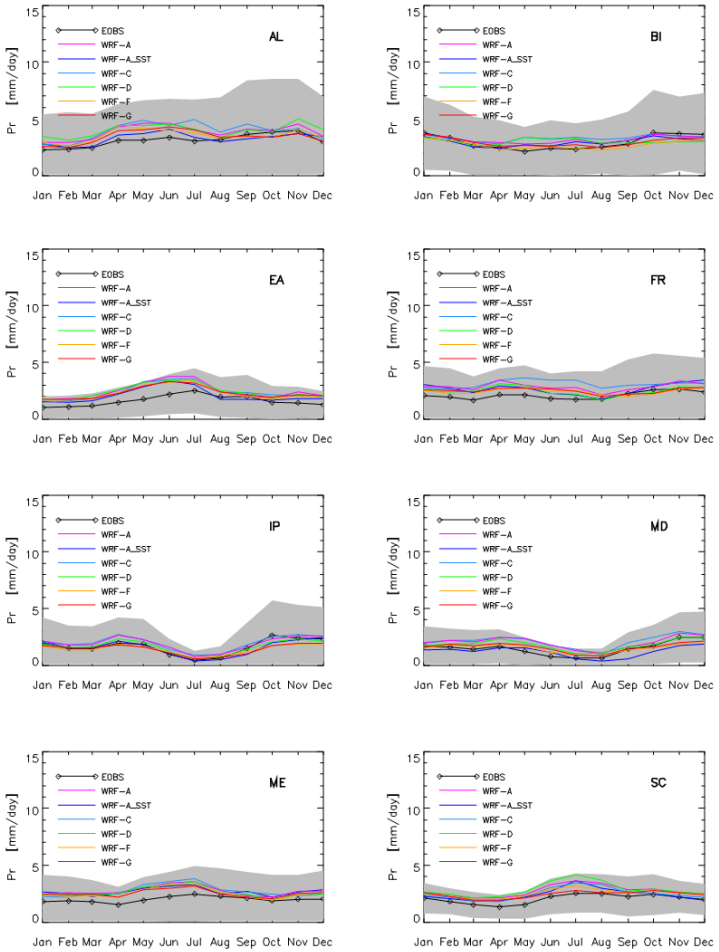

Figure 4. Mean precipitation annual cycle. The grey area indicates observational standard deviation.

GMDD
7, 6629–6675, 2014

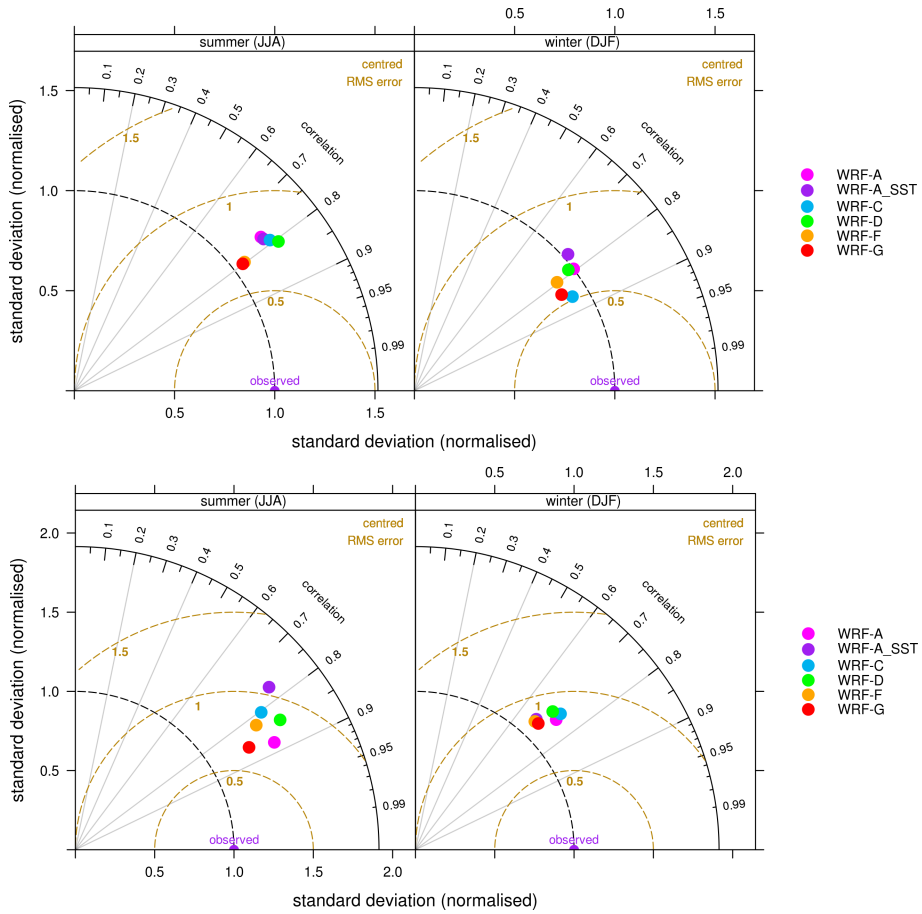

Figure 5. Temporal (upper panel) and spatial (bottom panel) Taylor plots for precipitation averaged over Europe for summer and winter 1990–2008.

GMDD
7, 6629–6675, 2014

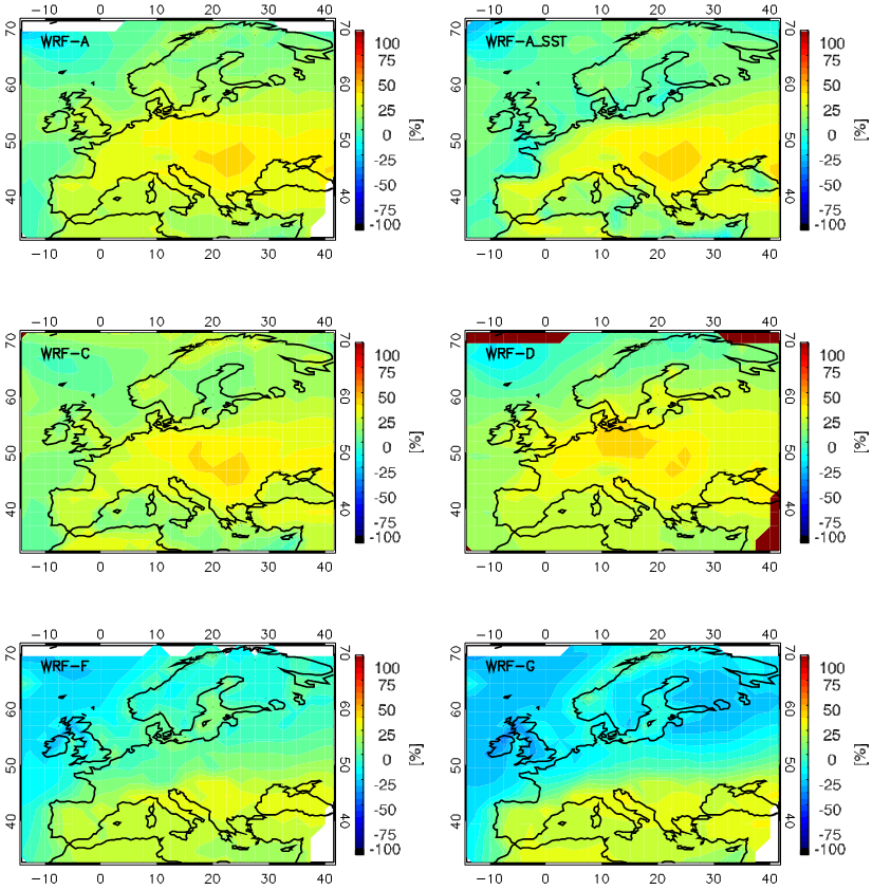

Figure 6a. Mean summer 1990–2008 downward surface shortwave radiation bias (WRF-ISCCP).

GMDD
7, 6629–6675, 2014

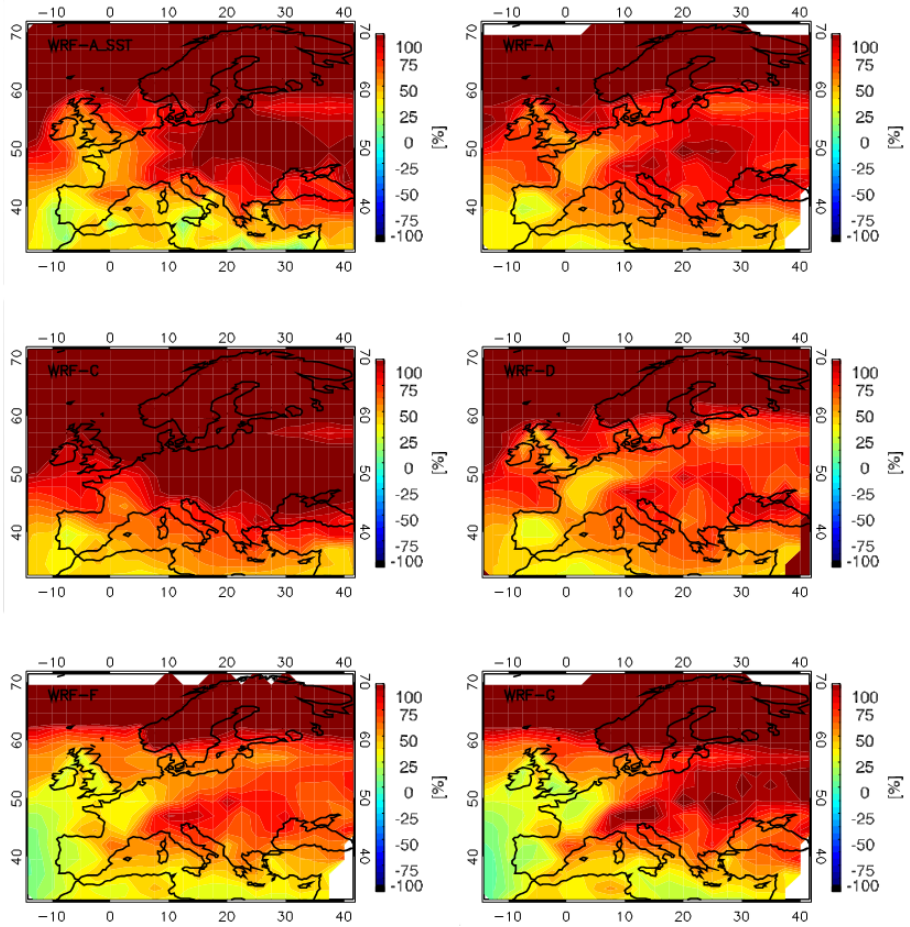

Figure 6b. Mean winter 1990–2008 downward surface shortwave radiation bias (WRF-ISCCP).

GMDD
7, 6629–6675, 2014

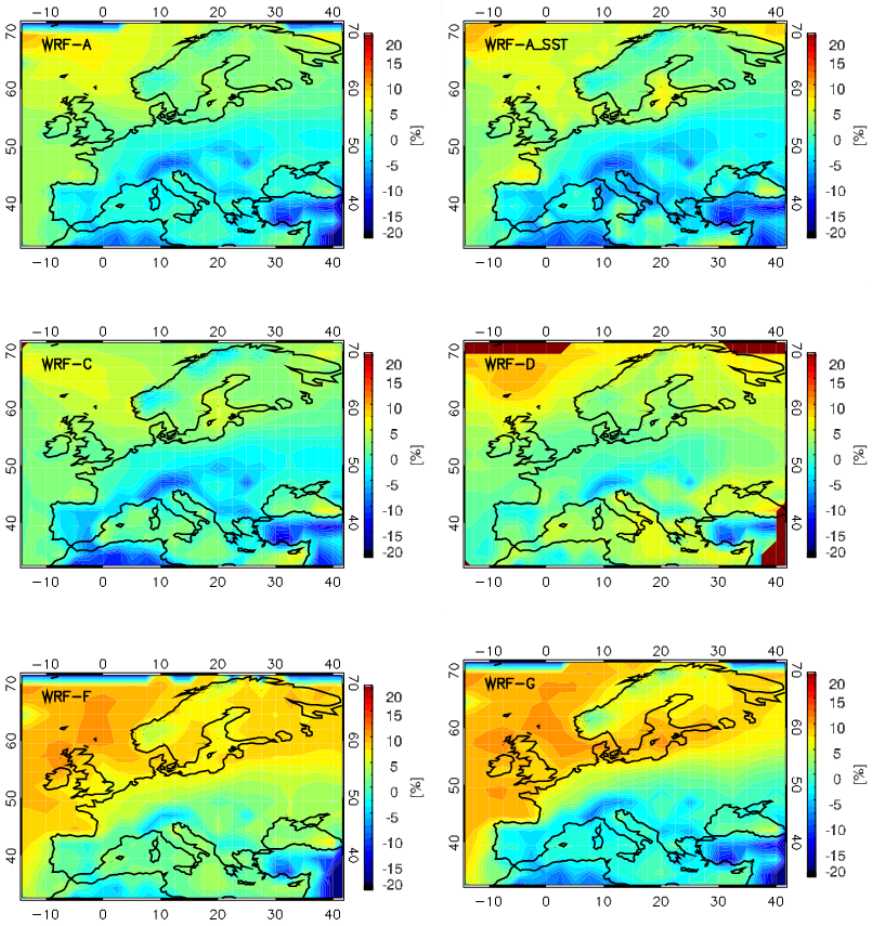

Figure 7a. Mean summer 1990–2008 downward surface longwave radiation bias (WRF-ISCCP).

GMDD
7, 6629–6675, 2014

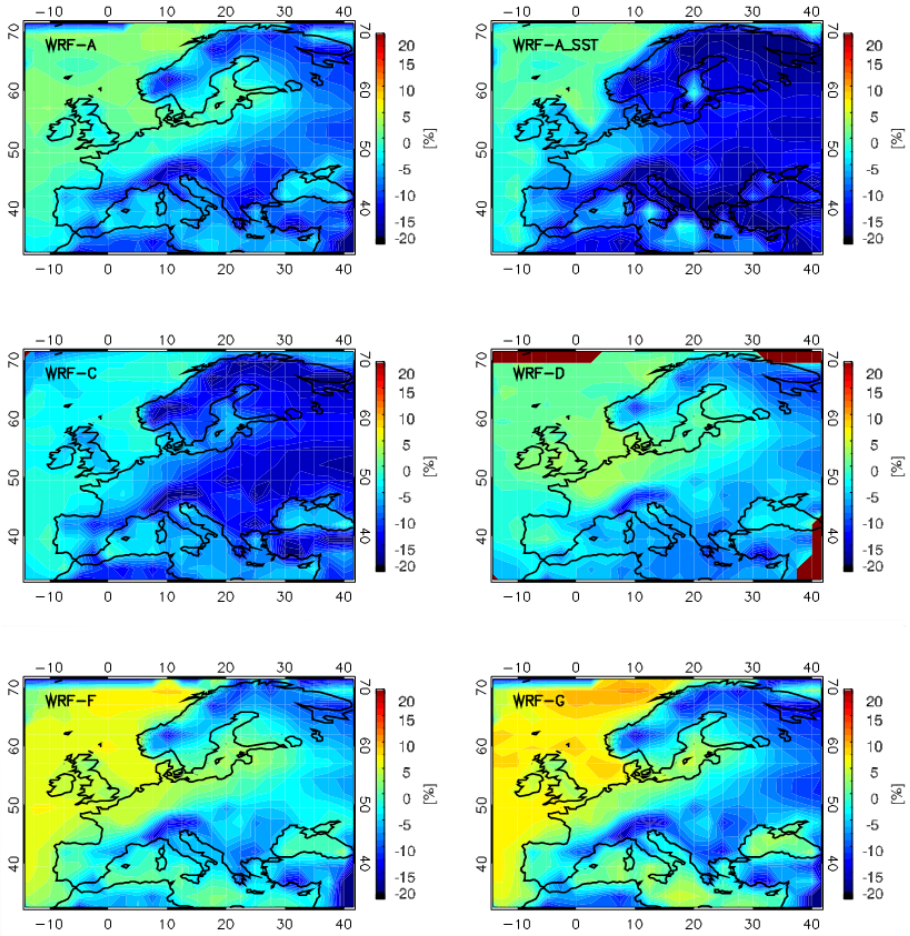

Figure 7b. Mean winter 1990–2008 downward surface longwave radiation bias (WRF-ISCCP).

GMDD
7, 6629–6675, 2014

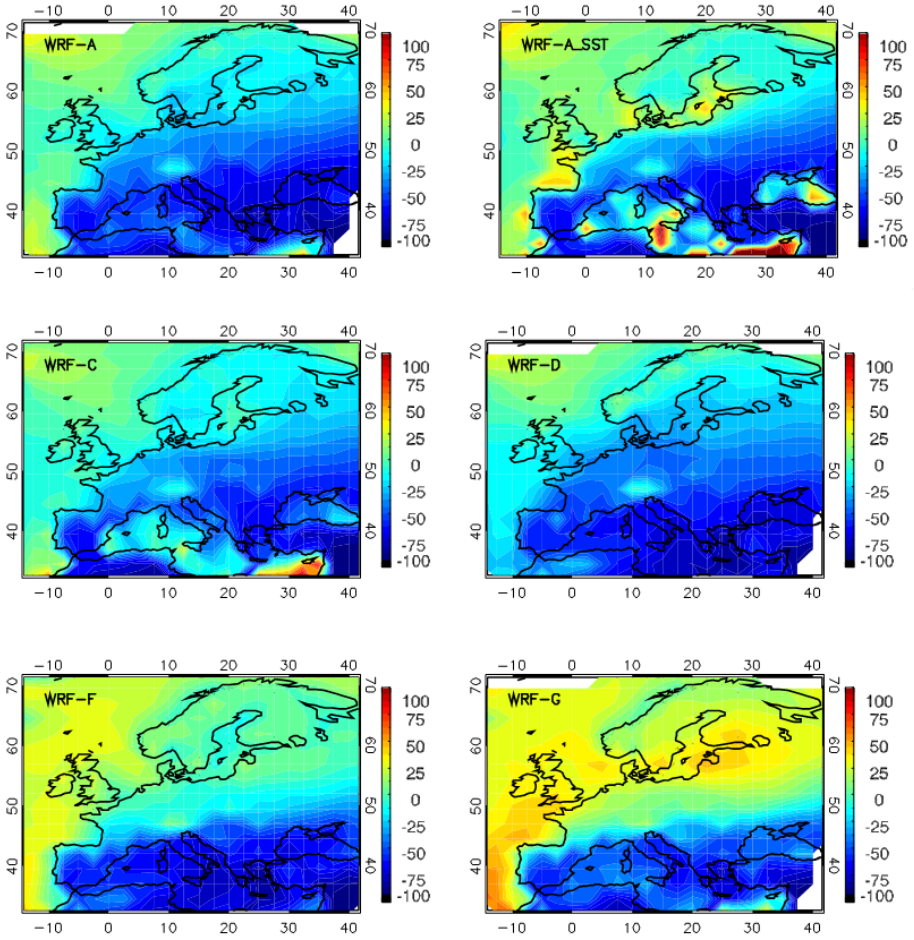

Figure 8a. Mean summer 1990–2008 total cloud cover bias (WRF-ISCCP).

GMDD
7, 6629–6675, 2014

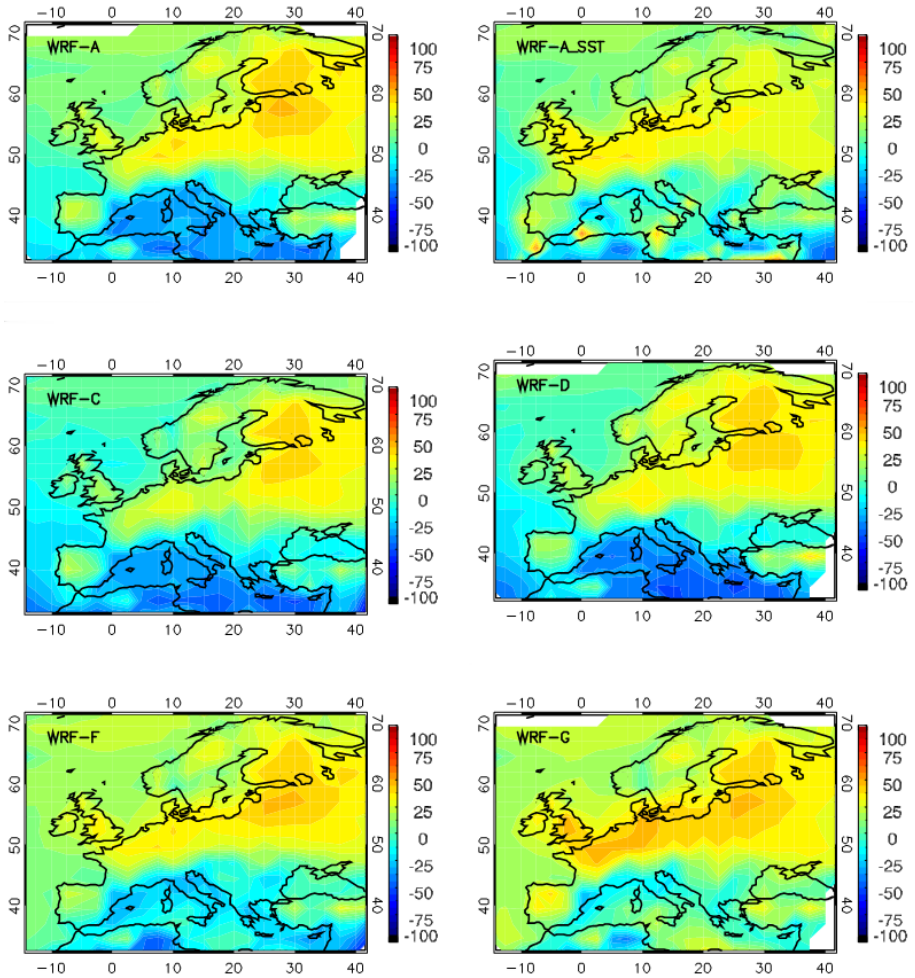

Figure 8b. Mean winter 1990–2008 total cloud cover bias (WRF-ISCCP).

GMDD
7, 6629–6675, 2014